2014

CHARACTERIZATION OF INDIVIDUAL CHARGED Au25(SG)18 CLUSTERS AND THEIR ENHANCEMENT OF SINGLE MOLECULE MASS SPECTROMETRY

Christopher Angevine
Virginia Commonwealth University

CHARACTERIZATION OF INDIVIDUAL CHARGED $Au_{25}(SG)_{18}$ CLUSTERS AND THEIR ENHANCEMENT OF SINGLE MOLECULE MASS SPECTROMETRY

A thesis submitted in partial fulfillment of the requirements for the degree of Master of Science in Physics and Applied Physics at Virginia Commonwealth University.

by

Christopher E. Angevine

B.S. Physics
B. S. Applied Mathematics

Virginia Commonwealth University, 2012

M.S. Physics

Virginia Commonwealth University, 2014

Director: Dr. Joseph Reiner, Assistant Professor, Department of Physics

Virginia Commonwealth University
Richmond, Virginia
May, 2014

Acknowledgments

I would like to thank Dr. Joseph E. Reiner for accepting me into his research group. He has been a well of knowledge and his mentorship has motivated me to continue to push myself. I would also like to thank my family for their never ending support and love. I would also like to thank my friends who have been in the grad school trenches, especially Alex Khammang and Brandon Child who have given me amazing advice throughout my time at VCU.

Table of Contents

List of Figures

Abstract

CHARACTERIZATION OF INDIVIDUAL CHARGED $Au_{25}(SG)_{18}$ CLUSTERS AND THEIR ENHANCEMENT OF SINGLE MOLECULE MASS SPECTROMETRY

By Christopher E. Angevine, M.S.

A thesis submitted in partial fulfillment of the requirements for the degree of Master of Science in Physics and Applied Physics at Virginia Commonwealth University.

Virginia Commonwealth University, 2014.

Major Director: Dr. Joseph Reiner, Assistant Professor, Department of Physics

Metallic quantum clusters are stable structures that can exhibit many useful magnetic, chemical, and optical properties. Developing clusters for specific applications requires accurate methods for characterizing their physical and chemical properties. Most cluster characterization methods are ensemble-based measurements that can only measure the average values of the cluster properties. Single cluster measurements improve upon this by yielding information about the distribution of cluster parameters. This investigation describes the initial results on a new approach to detecting and characterizing individual gold nanoclusters ($Au_{25}(SG)_{18}$) in an aqueous solution with nanopore-based resistive pulse sensing. We also present a new application where the clusters are shown to increase the mean residence time of polyethylene glycol (PEG) molecules within an alpha hemolysin (αHL) nanopore. The effect appears over a range of PEG sizes and ionic strengths. This increases the resolution of the peaks in the single molecule mass spectrometry (SMMS) current blockade distribution and suggests a means for reducing the ionic strength of the nanopore solute in the SMMS protocol.

Chapter 1:

Introduction

1.1 Overview

In the past decade nanoparticles have been receiving more attention in the scientific fields. This is due to their ability to possess useful mechanical, electrical, chemical, optical and magnetic properties that are not present in the bulk.[1] The synthesis of highly stable gold nanoparticles[2] has led to the creation of ligand protected clusters with a controllable number of atoms.[3] This allows the size of the clusters to remain stable with a small number of atoms and allows the clusters to retain their unique properties. These properties can be used to replace existing materials.[4]

One class of cluster that has been well characterized and understood is gold. The techniques used to characterize gold clusters are, mass spectrometry[5], electrochemistry[6], and electron microscopy[7]. These tests are excellent for bulk measurements but they all lack the ability to look at single molecules in their natural environment. Single cluster analysis would allow for a better understanding of the variability within a cluster population. Nanopore-based, sensing could allow for single cluster characterization.

There are two major branches of the nanopore community, biological nanopore systems and solid state nanopore systems. Solid state pores are usually made out of dielectric materials

such as SiN, Al_2O_3, or graphene.[8] Since the membrane partitioning the electrolyte in a solid state nanopore system is a dielectric and not a lipid bilayer (as is the case with biological nanopore systems) solid state pores have superior chemical and thermal stability over biological pores. However they are sensitive to the conditions they are created under which causes the pores to be difficult to reproduce[9,10] and lack the unique geometries that biological nanopores possess.[11] This study will utilize biological nanopores for single cluster analysis.

The nanopore system essentially operates like a nanoscale Coulter counter.[12] Small molecules, commensurate in size with the pore volume, enter the pore and reduce the flow of ionic current. This gives rise to measurable blockades that can be analyzed to extract information about the analyte. Nanopore sensing became a topic of great interest when in 1996, it was shown that a α-hemolysin (αHL) pore could be used to detect single stranded DNA (ssDNA) at the single molecule level.[13] Since then nanopore sensing has been used in applications such as, nucleic acid sequencing,[14] single molecule mass spectrometry,[14,15] and proteomics.[16] Rapid, accurate and affordable DNA sequencing has been a long standing problem and continues to motivate the development of nanopore sensors. One of the problems that have limited the ability to sequence DNA is the short times the DNA molecules spend inside the pore. This motivates the need to slow down the transit of DNA molecules through the pore. More generally, the ability to increase the residence time of any analyte, not just DNA, in the pore is a ubiquitous problem in nanopore sensing and has been the focus of several research groups as they have attempted to increase the residence time of many different types of molecules for improved nanopore sensing.

1.2 Motivation and current work

The work described herein focuses on the development of a reliable characterization method for water-soluble metal clusters and the application of metallic clusters to increase the residence time of charged analyte in a nanopore. Specifically, we study here $Au_{25}(SG)_{18}$ in solution with resistive pulse sensing using an αHL nanopore to estimate the size and charge of the clusters. We then use these charged clusters to increase the residence time of polydisperse polyethylene glycol (PEG) in an αHL pore.

PEG is an important tool for nanopore sensing because it has been shown to yield current blockade peak distributions with single monomer resolution.[14] This motivates the development of PEG as a single molecule nanopore label where molecules that are too small or spend too little time in the pore could be attached to PEG molecules for characterization purposes.[15,35] This motivates the development of improved detection of PEG molecules by the αHL pore and the cluster-increased residence time of PEG in the pore is shown to yield more highly resolved peaks in the PEG-induced current blockade distribution.

1.2.1 Characterization of single $Au_{25}(SG)_{18}$ clusters

This report describes initial results of a new approach to detecting and characterizing individual $Au_{25}(SG)_{18}$ nanoclusters, in an aqueous solution with nanopore-based resistive pulse sensing. Clusters enter through the *cis* side of an αHL pore and create both short and long-lived blockade events. The short time blockades allow for sufficient statistics to characterize the size of the clusters. We use the current blockades to estimate the size and charge of the clusters and the estimates are in reasonable agreement with previously measured values.[17]

1.2.2 Au clusters to enhance water-soluble single molecule mass spectrometry

Water-soluble metallic clusters have been used for a number of important applications. We present here a new application where these clusters are shown to increase the mean residence time of polyethylene glycol (PEG) molecules within an αHL nanopore. The effect appears over a range of PEG sizes and ionic strengths. This increases the resolution of the peaks in the single molecule mass spectrometry (SMMS) current blockade distribution and suggests a means for reducing the ionic strength of the nanopore solute in the SMMS protocol.

Chapter 2:

Background

Nanopore systems have several different designs depending on what is being studied. In this work nanopore sensing is similar to a nanoscale Coulter counter where ionic current blockades result from single molecules blocking the flow of ions through the pore. The current blockades can be analyzed to extract information about the analytes. Figure 1 is a schematic illustration of the nanopore sensing protocol. Each image shows a different analyte mixture that interacts with the nanopore and the corresponding current blockades that result from these mixtures. The left image represents a monodisperse solution of small molecules that will cause short-lived events that happen at high frequency. The middle image shows what could happen if some of the small molecules are bound to larger molecules. The frequency of short-lived events decreases in direct proportion to the number of small molecules that are bound to the larger analyte. The right image shows a long-lived blockade that result from the conjugate molecule entering the nanopore. The point of these illustrations is to demonstrate how the properties of the current blockades can be used to inform about the details of the molecules interacting with the pore. For the work described in this thesis, we use the well characterized alpha-hemolysin (αHL) pore for nanopore sensing.[18]

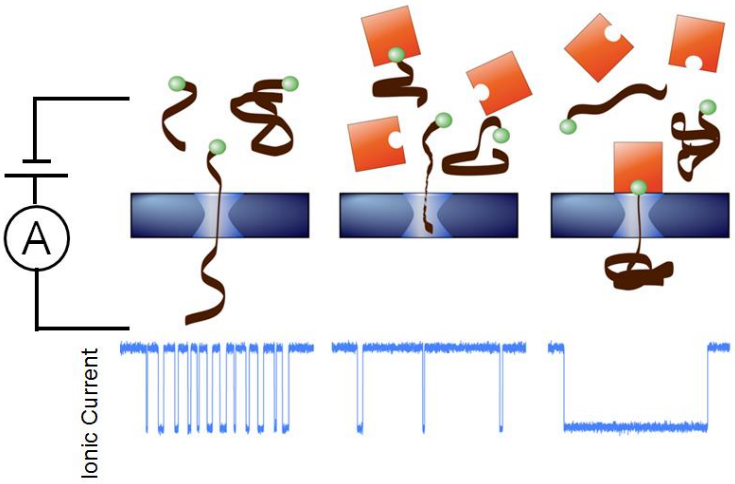

Figure 1: Blockade Representation: Principle of ionic current blockade nanopore detection. A nanoscale hole is formed in a membrane that separates two electrolyte solutions. A transmembrane voltage or concentration gradient is applied that drives ionic current through the hole. If the hole remains in an open conformation for extended periods, then single analyte molecules that enter the hole give rise to measureable current blockades. Three types of blockades are illustrated here that correspond to three different analyte configurations. Far left is for small molecules that enter and exit the hole giving rise to short lived blockades, center is a poly disperse mixture of molecular sizes where the concentration of small molecules is reduced which leads to a reduction in the frequency of blockade events and the right panel shows a blockade that corresponds to a large molecule entering and blocking the pore for an extended period of time. (Figure reproduced with permission from reference 11).

The work horse of the nanopore sensing community is the alpha-hemolysin pore. This pore is a transmembrane protein nanopore secreted by *Staphylococcus aureus*.[19] This protein is water soluble and made of seven repeat monomer subunits, which combine to form a heptameric prepore on the surface of the membrane. The pore assembles via an interaction with the lipid bilayer membrane where the stem portion of the protein extends across the membrane to form a nanoscale hole through the membrane.[20] Figure 2 represents a cross section of the nanopore showing the dimensions obtained through x-ray diffraction.[21] The αHL pore can be divided into two sections, the large vestibule on the *cis* side and the narrow lumen on the *trans* side. The vestibule region is about 3.6 nm across with a 2.6 nm opening to solution. The *trans* side of the

pore is approximately shaped like a right cylinder with an opening of 2.2 nm. There is a 1.5 nm pinch point between the two sections of the αHL pore formed from the side chains of Glu111, Lys147, and Met113.[20] Molecules entering from the *cis* and *trans* side of the pore give rise to different current blockade signatures, which is expected given that most of the voltage drop through the pore is concentrated in the *trans* side lumen see Fig 2B.[22]

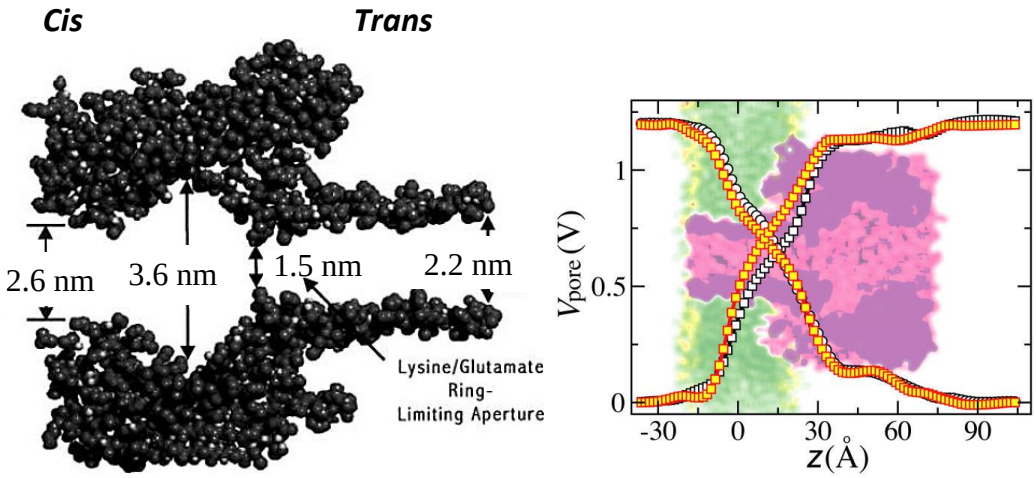

Figure 2: Dimensions and Properties of an αHL Pore: This is the dimensions of a single αHL pore. The large mushroom headed side is known as the *cis* side while the small tube is known as the *trans* side. (Figure 1B reproduced with permission from 23) Figure 2B represents the voltage drop across the αHL pore under positive and negative applied bias calculated with MD simulations at pH 8.0 (orange) and pH 4.5 (black). The steepest voltage drops are confined with the *trans* side stem of the pore and the Lysine/Glutamate ring separating the *cis* side vestibule from the stem. (Figure 2B reproduced with permission from reference 22).

The best molecules with which to perform nanopore sensing yield large current blockades that reside in the pore for extended periods of time (>100 μs). One molecule that satisfies this requirement in αHL nanopores is polyethylene glycol (PEG). PEG is a stable, easily modifiable molecule that does not bind or chemically interact with the αHL pore, but nevertheless, yields deep blockades (PEG 1500 yields 80% blockades) for extended periods of time (> 1ms) when

entering the pore from the trans side (see Figs. 3-5). PEG varies in size and the αHL nanopore can easily fit PEG molecules with up to 60 monomer repeat units.[14] It has been shown that by averaging the current blockades from PEG molecules, one can separate and resolve blockades at the single monomer level (see Fig. 4).[14]

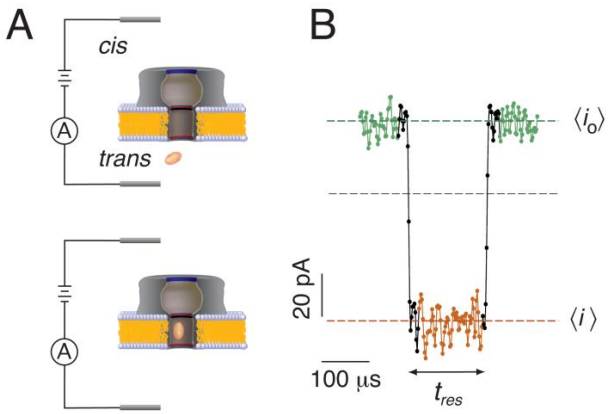

Figure 3: Single PEG Blockade Overview: Schematic illustration of nanopore detection of a single PEG molecule and the resulting current blockade. (A) A transmembrane voltage is applied across the nanopore and a single PEG molecule enters the *trans* side of the pore. (B) Upon insertion, a current blockade is recorded. The blockade depth is calculated from the ratio of the average current of the blockade <i> to the average current of the open state current before and after the blockade <i_0>. In addition, the residence time for each <i>/<i_0> blockade is recorded. (Figure reproduced with permission from reference **Error! Bookmark not defined.**)

It has also been shown that larger PEG molecules will stay in the αHL pore longer then smaller molecules.[14] In addition, the depth of the current blockade depends on the relative volume of the PEG to the volume of the pore.**Error! Bookmark not defined.** The difference in this ratio for PEG molecules than differ in size by a single monomer is approximately 1% and therefore, it is possible to average the current blockades and separate PEG molecules that differ in size by a single monomer unit. This is done by creating a histogram of all the current

blockades for a sample of PEG molecules. Figure 4 shows this distribution where each peak corresponds to uniquely-sized PEG molecules with *n* monomer repeat units. The peak from current blockades originating from a monodisperse mixture of PEG with a fixed n value (n=29) are superimposed on the polydisperse distribution to show how the peaks are calibrated by monomer repeat unit.

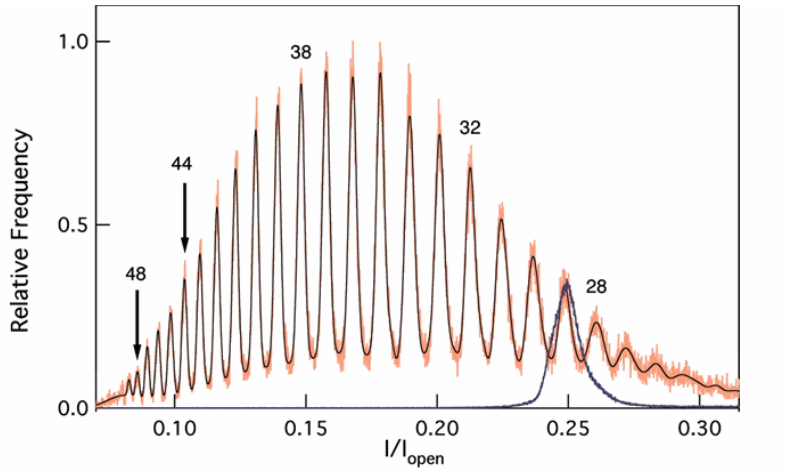

Figure 4: PEG Comb Overview: Current blockade distributions for a polydisperse and monodisperse mixture of PEG molecules as measured by a single αHL nanopore. The blue line represents monodisperse PEG-28. The red comb is a polydisperse mixture of PEG 1500. The clear peaks represent a single repeat unit, n, with a weight of ~44.053 g/mol. The solid black line is a Gaussian mixture model fit to the polydisperse mixture. As the polymer repeat number increases, the blockade depth gets deeper. (complete blockade corresponds to a zero value on the horizontal axis) (Figure reproduced with permission from reference 11)

The separation in PEG blockades into each respective peak allows one to analyze the residence time distribution of a given *n*-sized polymer. The residence time distribution for an n-sized PEG molecule in the αHL pore is shown in Fig 5A. The residence time distribution is well described by an exponential offset function, $P(t) = P_0 + A\exp\left(-t/\langle\tau_n\rangle\right)$ with mean residence

time $\langle \tau_n \rangle$. It has been shown previously that the mean residence is well described with an Arrenhius-like free energy barrier model with $\langle \tau_n \rangle = \tau_0 \exp\left(\Delta G(n,V)/k_B T\right)$.[15] Where τ_0 is the barrier-free diffusion residence time, n is the number of repeat units in the PEG molecule, $k_B T$ is the Boltzmann temperature term and $\Delta G(n, V)$ is the voltage and PEG-size dependent free energy barrier that must be overcome to drive a PEG molecule through the pore. [15] This equation has been used to describe the mean residence time for a range of PEG molecules under different applied voltages as seen in Fig 5B. If the molecule becomes too large or small then it will be too difficult to detect because the molecule will spend too little time in the pore in the nanopore sensor to be detected at the bandwidth of the system (10 kHz).

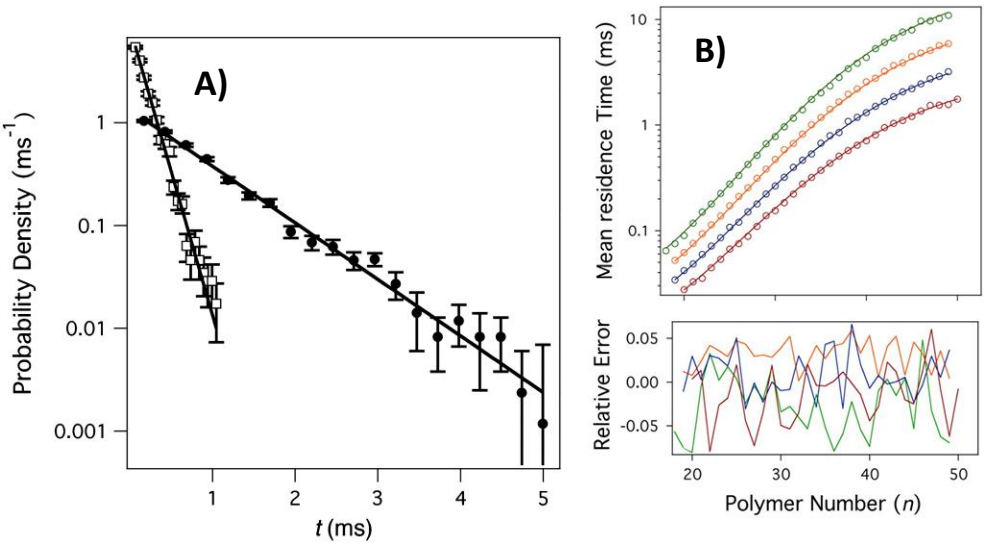

Figure 5: Residence Time distributions and mean residence time depend on the applied voltage and polymer size: A) Mean PEG residence times for each peak in the current blockade distribution. The squares have an applied voltage of -70mV and the circles are an applied voltage, -40 mV. B) Each peak is assigned a polymer repeat number, n, by calibrating with a monodisperse mixture of PEG with a known n-value. The mean residence times result from least-square fitting with an exponential offset function $A\exp(-(t-t_0)/\tau)$, where τ is the mean residence time of the PEG in the pore. It is clear that molecules spend greater time in the pore. (Figures reproduced with permission form reference 15)

It is evident from Fig. 5 (right) that as PEG molecules become larger, the time they spend in the pore increases. Increasing the residence time of molecules in the pore is a long standing problem in the nanopore sensing community[24] because it would improve the accuracy of blockade current measurements. This calls for new methods to see if there is an easy and effective way to extend the range of nanopore sensing to smaller and larger molecules by increasing the molecules residence time in the pore.

Chapter 3:

Characterization of $Au_{25}(SG)_{18}$ Within a Nanopore Detector

3.1 Background of the $Au_{25}(SG)_{18}$ Cluster

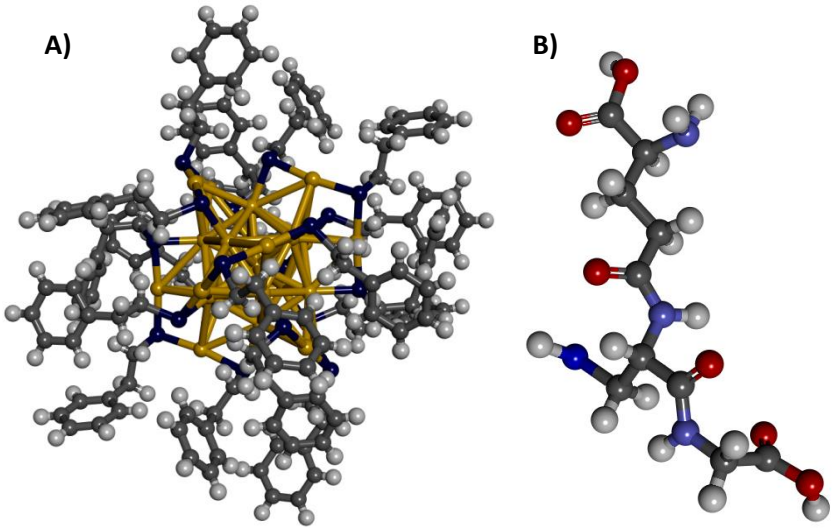

Figure 6: $Au_{25}(SG)_{18}$ and Glutathione: A) The structure of $Au_{25}(SCH_2Ch_2Ph)_{18}$ this structure is used in x-ray diffraction to find the structure of the gold cluster core.**Error! Bookmark not defined.** B) The structure of a single glutathione ligand.[25] This ligand replaces the $-(CH_2Ch_2Ph)$ ligand connecting at the sulfur. (Structure obtained from PDB)[26] (Legend: Dark Blue = Sulfur, Light Blue = Nitrogen, Yellow = Gold, Dark Grey = Carbon, White = Hydrogen, Red= Oxygen)

Nanoparticles come in many shapes, materials, and sizes. $Au_{25}(SG)_{18}$ is a ligand stabilized cluster. It is formed by taking Au_{13} clusters and stabilizing them with four Au_3S_2 "staples".[27] These move the lack of electrons to the sulfur, from here we have a lot of options. Depending on the ligand that is attached to the sulfur can change the properties of the cluster. Figure 6a shows a crystal structure of $Au_{25}(SCH_2Ch_2Ph)_{18}$.[17] Figure 6b is shows the structure of

glutathione, which can be attached to the gold cluster on the 18 sulfur points. The glutathione ligands make the cluster water soluble. Developing applications for $Au_{25}(SG)_{18}$ is difficult because the size and charge of these clusters have not fully been characterized through experimental measurements or theoretical calculations. Given the pKa values for the glutathione ligands are 1.94 for a strong acid and 9.22 for a strong base[28] it is expected that these clusters are negatively charged in near neutral pH conditions. Also, TEM images show that dried $Au_{25}(SG)_{18}$ clusters are about 1.2 – 1.5 nm in diameter.[29]

A need exists to develop an accurate tool for characterizing water-soluble metallic clusters so the size and charge distributions of these clusters in solution can be measured. With these measurements it should be possible to improve theoretical calculations[17,27] describing the structure of these clusters with the overall goal of developing new novel functions. In this chapter of the thesis we demonstrate that nanopore sensing can be used to measure the size and charge of water-soluble metallic clusters.

3.2 Experimental Set-up

Setup: Attach a 1 cm^2 PTFE (teflon) sheet with PDMS (Kwikset, WPI) with an approximately 100 μm hole in the center onto a previously fabricated large teflon holder. The teflon sheet is positioned approximately 100 μm from the top of a microscope cover slip mounted onto a homemade holder that sits on an inverted microscope (Axio Observer D, Zeiss, Germany). Apply 1 μL of a pre-paint mixture of 0.5 mg/ml DPhyPC (1,2 diphytanolyl-*sn*-glycero-3-phosphatidylcholine; Avanti Polar Lipids, Alabaster, AL) dissolved in pentane around the hole. After the prepaint mixture dries (≈ 5 min) the lower chamber, which contains a Ag/AgCl bare electrode wire, and the upper chamber are filled with an electrolyte solution (1M

KCl, 10 mM Tris, pH 7.2, all chemicals unless otherwise noted were purchased from Sigma Aldrich, St. Louis MO). For *trans* entry studies, $Au_{25}(SG)_{18}$ is added to the lower chamber to a final concentration of 4 μM. The top chamber contains a patch pipette formed with a laser based puller (P-2000, Sutter Instruments, CA) that contains matching 1M KCl buffer and a Ag/AgCl bare electrode wire. For *cis* entry experiments, the patch pipette is filled with $Au_{25}(SG)_{18}$ to a final concentration of 25 μM.

Membrane formation and single channel patching: A glass microcapillary (femtotip II, Eppendorf, NY) is positioned with a motorized manipulator (MPC-275, Sutter Instruments, CA) ca. 100 micron above the hole in the teflon partition. Several picoliters of 10 mg/ml DPhyPC:hexadecane solution is ejected from the tip and adhered to the teflon surface. A glass rod with a glass ball formed at the end wipes the lipid across the hole. The lipid/solvent mixture thins over a period of several seconds and a lipid bilayer membrane is formed and verified by optical microscopy. A second glass microcapillary containing 50 μg/mL of αHL (List Biological, CA) is positioned a few microns from the bilayer membrane surface and a small backing pressure (~ 20-50 hPa) is applied (Femtojet, Eppendorf, NY) for a period of tens of seconds. A transmembrane potential (typically 10 mV) is applied to verify the insertion of several hundred αHL pores. When a sufficient number of pores span the membrane, the backing pressure is turned off and the αHL capillary is removed from solution. The borosilicate patch pipette tip is brought down in contact with the membrane via a motorized manipulator to form a patch membrane across the tip. If the membrane contains 0 or more than 1 channel, as measured by the current (single channel conductance ≈ 1 nS), the tip is lifted off the bilayer membrane and a backing pressure is applied to remove the patch membrane and the process is repeated until a single αHL channel is localized within the patch area. The current is recorded with an amplifier

(Axopatch 200B, Molecular Devices, CA), sampled at 50 kHz (Digidata 1440A, Molecular Devices) and low-pass filtered with a 4-pole 10 kHz Bessel filter. We observe a slight drift in the current reading (~0.1 pA/min) from the unprotected electrodes that is corrected before each data trial.

Synthesis of $Au_{25}(SG)_{18}$ in water 100 mg of $HAuCl_4$ (0.253 mmol) was dissolved in 50 mL of DI water resulting in a yellow solution. 307 mg of glutathione (1.00 mmol) was slowly added to the gold salt under slow stirring, while the yellow solution changed to a cloudy white suspension. Next the solution was cooled in an ice bath for 30 minutes. After 30 minutes, 94.6 mg of $NaBH_4$ (2.5mmol) was dissolved in 12.5 ml of ice cold DI water and added to the mixture all at once while stirring at 1000 rpm. The milky white color of the mixture rapidly turned black after the addition of $NaBH_4$ indicating the formation of nanoparticles. After 1h the mixture was rotary evaporated until total volume was reduced to 5 mL, while the temperature was kept below 30 ^{0}C. Then 20 mL of methanol was added to the product mixture and centrifuged for 3800 rpm for 3 minutes. The resulting precipitate was washed 3 times with methanol. $Au_{25}(SG)_{18}$ and $Au_{38}(SG)_{24}$ were obtained using polyacrylamide gel electrophoresis (PAGE) as described previously.[30] We only report nanopore analysis here on the $Au_{25}(SG)_{18}$ particles.

3.2.1 Data Analysis

Analysis of the current traces was performed with Igor 6.2 (Wavemetrics, Oregon) (all points histograms), Clampfit 10.1 (Molecular Devices) (I-V curves) or Labview 8.5 (National Instruments, TX) (residence time and blockade event analysis). A threshold algorithm described previously[15] was used to calculate the average blockade depth and residence time for each event. A current blockade was counted whenever the current was less than 80% of the full long time (~1 min) open channel current for a minimum of 120 μs. In addition, the open state was only

calculated before each blockade event rather than averaged from before and after. This eliminated artifacts from trapped state events that required switching of the voltage polarity to remove the cluster from the pore. Residence times were only calculated for events were the cluster spontaneously escaped from the pore without the aid of the polarity switch.

3.3 Results

3.3.1 Trace Analysis of a Single $Au_{25}(SG)_{18}$ Cluster

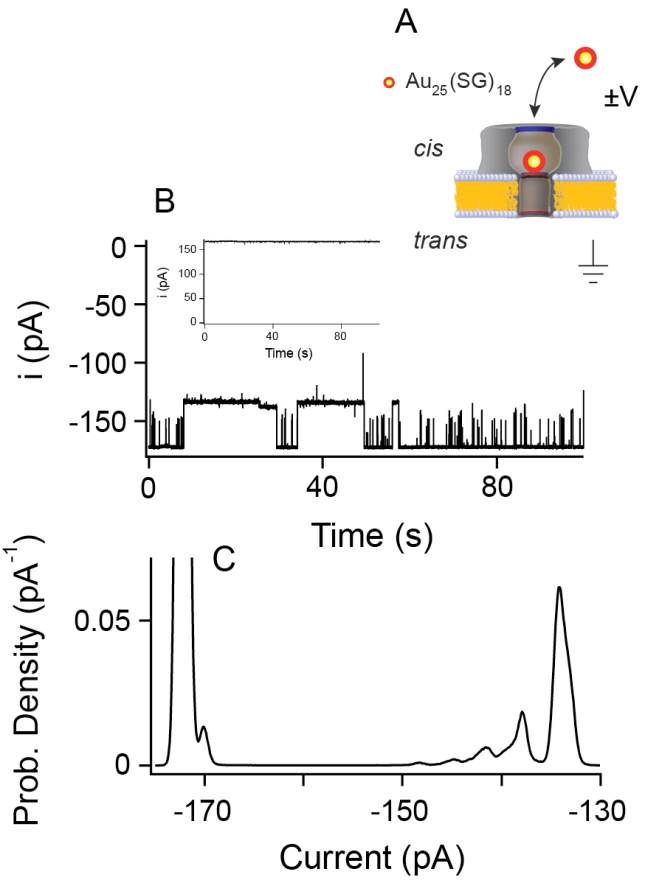

Figure 7: $Au_{25}(SG)_{18}$ Trace Analysis: Nanopore sensing of $Au_{25}SG_{18}$ clusters in 3.5 M KCl. (A) Clusters entering randomly into the nanopore. For presentation purposes, the data in this figure was filtered with a 100 Hz low-pass Hanning filter. (B) Filtered current trace of the $Au_{25}SG_{18}$ of -50mV. The inset shows the result with a V = +50mV transmembrane potential applied. The lack of blockades with a positive applied voltage indicates to show that the $Au_{25}SG_{18}$ are charge depended and can be driven into the pore. (C) The all points histogram of the negative voltage showing the quantized states of the gold particles.

Figure 7A shows an illustration of the experimental setup and the method of detection for -50mV applied across the membrane in a 3.5M KCl solution. This voltage and salt concentration provides clean well defined blockades that are easy to identify. The αHL pore is sitting in the unsupported lipid bilayer. The clusters diffuse in the *cis* side solution and randomly enter the pore under an applied voltage. Figure 7B shows short and long-lived current blockades from gold clusters entering and exiting the pore under a negative applied voltage (relative to the *trans* side of the pore). The open state for the applied -50 mV is i_{open}(-50mV) = (-172.3 ± 0.6) pA. The short lived-events could be used to characterize the gold clusters.[11] The inset to Fig. 8B, under a positive applied potential, the open state current is i_{open}(+50mV) = (165.8 ± 1.0) pA and no blockades are seen. This verifies that the clusters are negatively charged. The absence of blockades verifies that the clusters are negatively charged. The size of the blockades is small ($i_{block}/i_{open} \approx 0.75$) and leaves sufficient dynamic range for detecting other analytes while a cluster is in the *cis* side of the pore.

Figure 7C is an all points histogram of the trace. This shows where the current is most likely to be at any particular moment. The peak at i_{open}(-50mV) = (-172.3 ± 0.6) pA is the open state where there are no clusters. The peaks between $|i|$ = (130 – 150) pA suggest that the clusters are not a monodisperse as once thought. However due to the electrospray ionization mass spectrometry done on the clusters, by the group who produced the clusters, shows that the clusters are highly monodisperse. A least-squares fit to the largest blockade peak yields i_{block} = -(133.7 ± 1.1) pA. Therefore the different blockade states between $|i|$ = (130 – 150) pA could result from different sized cluster isomers[31], the cluster residing in different parts of the pore[32] or cluster induced modifications to the nanopore volume.[18,33] Future studies are required to address this issue.

3.3.2 Residence time of a Single $Au_{25}(SG)_{18}$ Cluster

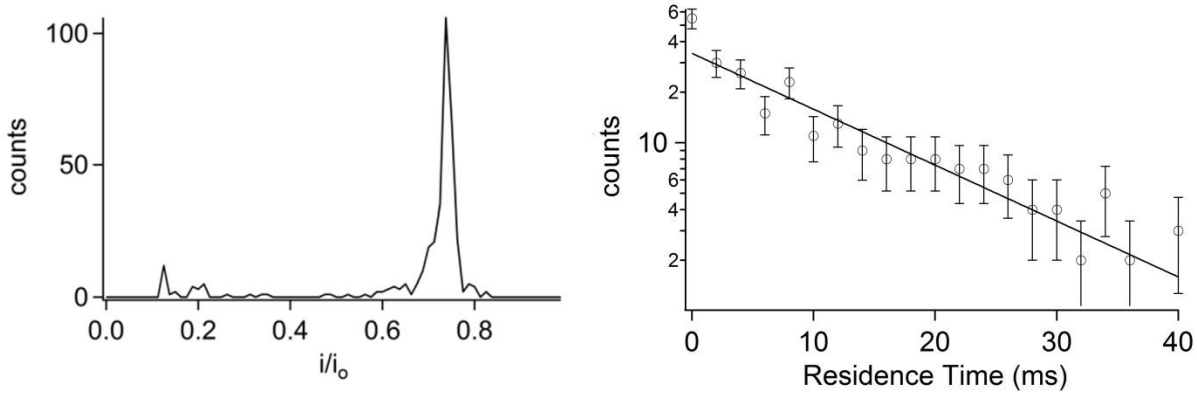

Figure 8: Single $Au_{25}(SG)_{18}$ Cluster Residence Time: Current blockade and residence time distributions for clusters entering the *cis* side of the nanopore under 100 mV applied potential. (*left*) Blockades give rise to a large peak with shallow blockades at $i/i_o \approx 0.75$ and two smaller peaks corresponding to deeper blockades at $i/i_o \approx 0.13$ and 0.20. The large number of shallow blockades may provide an accurate means for sizing the clusters while the long lived "trapped" states at 0.13 and 0.20 may be indicative of different orientations of the cluster within the nanopore. (*right*) The residence time distribution is well fit with a single exponential function with an average residence time of $t_{res} = (13.1 \pm 1.1)$ ms. The current trace for the data shown here lasted 1400 seconds and led to 353 blockade events.

Now that we have a better understanding of what will happen to the current when $Au_{25}SG_{18}$ interacts with the pore, figure 8 looks at the blocks created by the gold cluster blockades. The left image in figure 8 is the analysis of looking at each individual blockade, finding the average blockade depth, than plots it to see what depth is most prevalent. We see that the $Au_{25}(SG)_{18}$ blockade is most likely to be depth of $i/i_o \approx 0.75$. This means when a cluster enters the pore it will block about 25% of the current. This leaves plenty of room for the analyte to travel around the cluster and possible smaller molecules. We also see several smaller peaks around $i/i_o \approx 0.13$ and 0.2. These blockades represent very deep blocks, this may be caused by a smaller sized gold isomer[31] or the gold particle may have oriented itself to become lodged in the pinch point. The right image of figure 8 looks at the individual gold blockade events and finds

the time they spent in the pore. We graphed this using a logarithmic scale and the average residence time, *t, is* (13.1 ± 1.1) ms. In the nanopore community this is a very long time considering most PEG evens last only a few fractions of a millisecond.[15] This opens the possibility for using nanopores as a tool to characterize clusters.

3.3.3 Sizing a Single $Au_{25}(SG)_{18}$ Cluster

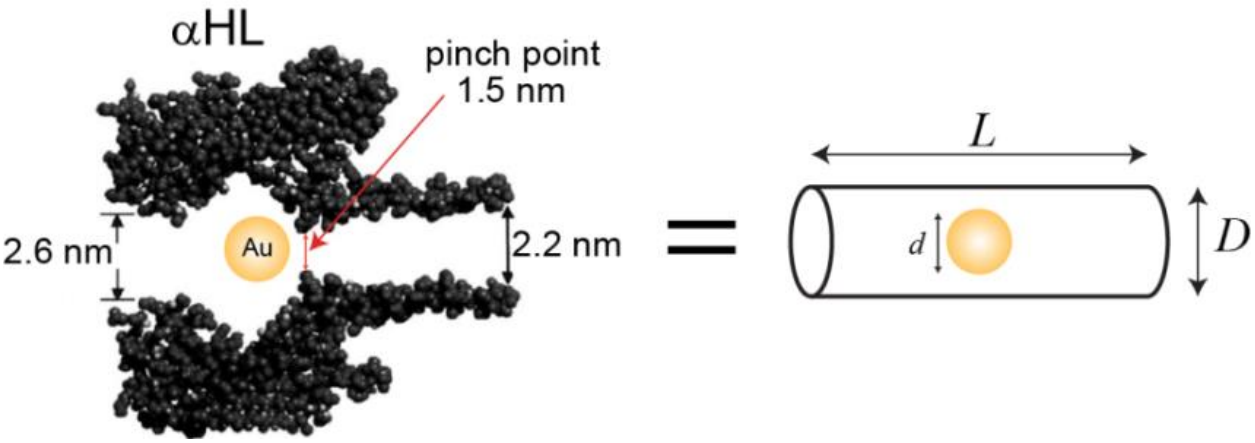

Figure 9: Sizing of a Single $Au_{25}(SG)_{18}$ Cluster: The gold cluster enters the pore from the *cis* side and yields a single current blockades. The nanopore is modelled with s a cylinder to make the calculation easier to derive. The known dimensions of the nanopore are, pore length(L) = (6.5 ± 1.5) nm = pore length, and pore diameter(D) = (1.9 ± 0.2) nm = pore diameter. The cluster blockade depth for the largest peak is, $\langle i \rangle / \langle i_o \rangle$ = 0.78 as shown in Figure 9. From Eq. 3.3 we find the diameter of the cluster is, d = (1.6 ± 0.1) nm.

We can estimate the size of the clusters from the depth of the current blockades. DeBlois and Bean derived an expression to size particles that block the flow of ionic current through a cylinder by assuming the particle's presence in the cylinder changes the ionic resistance. If you assumes the ionic resistivity in the pore is constant with and without the particle present then the resistance of the cylinder is given by,[12]

$$R = \rho \int \frac{dz}{A(z)}. \qquad (3.1)$$

where ρ is the resistivity of the fluid, and $A(z)$ is the cross sectional area of the cylinder where the sphere resides. The resistance with and without the particle present in the pore can be derived from Eq. 3.1. For the empty pore case, $A(z) = A_{pore}$ and Eq. 3.1 simplifies to R_0. As the cluster enters the pore the resistance is increased to R and $A(z)$ becomes a function of the cluster diameter. Substitution of this into Eq. 3.1 and integrating over the length of the pore from 0 to 10nm leads to and expression for $\Delta R = R - R_0$[34]. This we get,

$$\Delta R = \frac{4\rho}{\pi D}\left[\frac{\sin^{-1} x}{\sqrt{1-x^2}} - x\right], \text{ where } x = \frac{d}{D}. \tag{3.2}$$

Using Ohms law we rewrite this equation to get the ratio of the average current blockade over the average open state. We relate ΔR and $\frac{\langle i \rangle}{\langle i_0 \rangle}$ by holding voltage constant and solving for the resistance of a complete blockade,

$$\frac{i}{i_0} - 1 = \frac{i - i_0}{i_0} = \frac{\frac{V}{R} - \frac{V}{R_0}}{\frac{V}{R_0}} = \frac{R_0}{R - R_0} = \frac{R_0}{\Delta R} \tag{3.3}$$

Plugging in ΔR into Eqn. 3.3 and using the average open and blockade currents to get our final form,

$$\frac{\langle i \rangle}{\langle i_0 \rangle} = \left(1 - \frac{d}{L}\left(1 - \frac{\sin^{-1} x}{x\sqrt{1-x^2}}\right)\right)^{-1}, \text{ where } x = \frac{d}{D}. \tag{3.4}$$

We know from earlier experiments the dimensions of a nanopore from the values in Fig. 9, we substitute the following parameters into Eq. 3.3 to arrive at a value for the diameter of the $Au_{25}SG_{18}$ clusters $d = (1.6 \pm 0.1)$ nm. It appears the size of the nanoparticle is larger than the

pinch point of the αHL pore. This may explain the long-lived blockade events seen in Fig. 8B. Further analysis on the substructure of the current blockades could lead to a deeper understanding of any size distributions within the clusters as discussed about figure 8.

In addition to the size of the cluster, we can use nanopore detection to estimate the charge of the clusters. Assuming an exponential barrier must be overcome to drive a cluster into the pore, we employ an Arrenhius rate law $r = A\exp(D_E/kT)$ and note that $D_E = E_0 + qV$. Measuring the on-rate of clusters to the pore under different applied transmembrane potentials allows one to estimate the mean charge of the clusters. Fig. 10 shows the on-rate of clusters to the pore as a function of applied voltage fit with the exponential Arrenhius rate law. From the fit we estimate the charge of the cluster to be 3.2 ± 0.8 e.

3.3.4 On-Rate of $Au_{25}(SG)_{18}$

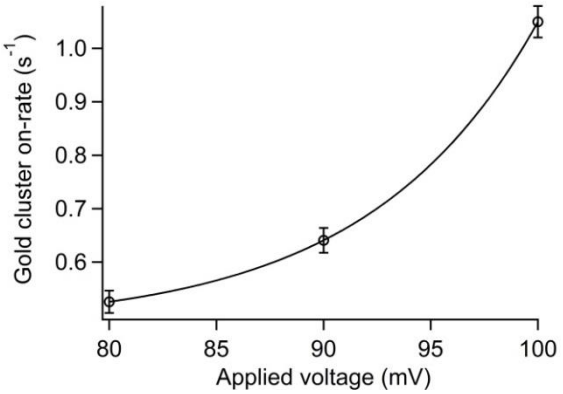

Figure 10: On-rate of a Single $Au_{25}(SG)_{18}$ Cluster: The $Au_{25}(SG)_{18}$ cluster on-rate to the αHL pore. The solid line shows the best-fit with an offset exponential function ($r = r_0 + A\exp(B(V-V_0))$). The growth constant of the function is B = 7.9 ± 2.0 meV. Substituting this value into the Arrenhius rate law leads to a value for the cluster charge of 3.2 ± 0.8 e. This data was recorded in 1 mol/L KCl solution with pH 7.2.

The on-rate will tell us how likely the cluster will be blocking the current versus the pore being in the open state. When a cluster enters the pore, the current is reduced as seen by the short and long-lived current blockades. The average on-rate for the clusters to the pore is $k_{on}(-50mV) = (0.12 \pm 0.01)\ s^{-1}$. Since the cluster is charged the higher the voltage is applied the more likely the cluster will go into the nanopore causing a blockade. After 70mV the chance of a charge nanoparticle being in the pore is greater than the cluster not being in the nanopore. Therefore a cluster has a chance of being caught in the vestibule of a pore for an almost indefinite amount of time. This makes it ideal an ideal situation for single molecule analysis and interactions.

Characterizing the clusters is important because we need to know the physical properties to better understand their structure which in turn can improve calculations. Future work will focus on other clusters, with different charges, varying sizes, and clusters made from different materials. We can then attempt to extract relevant information about the clusters, charge of the clusters, and cluster analyte interactions.

Now that we can characterize the nanoclusters we can attempt to use the clusters to see if they have an effect with other molecules. PEG is a great molecule to test to see if interactions will happen between the negatively charged cluster and the positively charged PEG. There may exist an interaction that enhances or quenches the blockades.

Chapter 4:

Experimental Procedure, Results, and Discussion of Enhanced Single Molecule Mass Spectrometry via Charged Metallic Clusters

4.1 Experimental Setup

The changes in the original setup, stated in Chapter 3, is we added a mixture of Poly dispersed PEG solution containing 3.5 mol/L KCl pH 7.2, 7.5 µmol/L of PEG 1000, 7.5 µmol/L PEG 1500 (Sigma, St. Louis, MO) and 1.5 µmol/L of monodisperse PEG 28 (Polypure, Oslo, Norway)to both top and bottom chambers of KCl to obtain a comb. For all other salt concentrations we used a 5µM Peg 28 concentration.

4.1.1 Data Analysis

Data analysis of the .abf files was performed with in-house software written in Labview 8.5 (National Instruments, Austin, TX). A threshold algorithm described previously**Error! Bookmark not defined.** was used to calculate the average blockade depth and residence time for each event. The average blockade depth associated with the gold clusters from Fig. 11 appears to be around 25%. Therefore, to avoid confusing gold cluster blockades with PEG induced blockades, the current blockade threshold was set to 35% above the open-pore current for 100 µs. This allowed analysis of current blockades from both the open nanopore state and the gold blocked state for the same pore. The average current for each blockade was normalized by the

average open current 1 ms before and 1 ms after that blockade and histograms of these open states were compiled. Events were discarded if the averaged open state current fell outside a narrowly defined window.

The residence time for each event was recorded and assigned to a particular PEG *n*-value based on the normalized blockade depth for the event. Ten-bin histograms (automatic bind widths) were calculated for the residence times for each *n*-sized PEG using the analysis package in IGOR 6.22A (Wavemetrics Inc. Lake Oswego, OR). Single offset exponentials were used to perform weighted fits of each residence time distribution. All reported error bars are ± 1 standard deviation.

The resolution for the *n*th peak in the current blockade distributions was calculated by $R_n = 1.18\ (\mu_n - \mu_{n+1})/(F_n + F_{n+1})$ where μ_n and F_n correspond to the mean and full width half maximum (FWHM) of the *n*th peak in the current blockade distribution respectively. The mean and FWHM values were found from a multipeak Gaussian fit to each current distribution using the Multipeak Fitting 2 package in IGOR.

4.2 Results

Since PEG and $Au_{25}(SG)_{18}$ are oppositely charged there may be some interaction, weather it is chemical or physical. We start with a cursory look at the trace files to see if there are any obvious changes to the open state with PEG and the gold blocked state with PEG.

4.2.1 PEG and $Au_{25}SG_{18}$ Trace Analysis

Figure 11A shows the open state with the PEG entering the pore through the *trans* side with no gold cluster present producing a deep blockade, $i_{PEG}/i_{open} \approx 0.35$, that is short lived. Figure

11B shows a gold blockade, entering from the *cis* side of the pore, which has an average depth, at -50 mV, of -136.5 ± 2.6 pA similar to Figure 7C. Some interaction occurs, either physical or chemical, which causes the PEG molecule, that is entering through the pore through the *trans* side, to increase the translocation time.

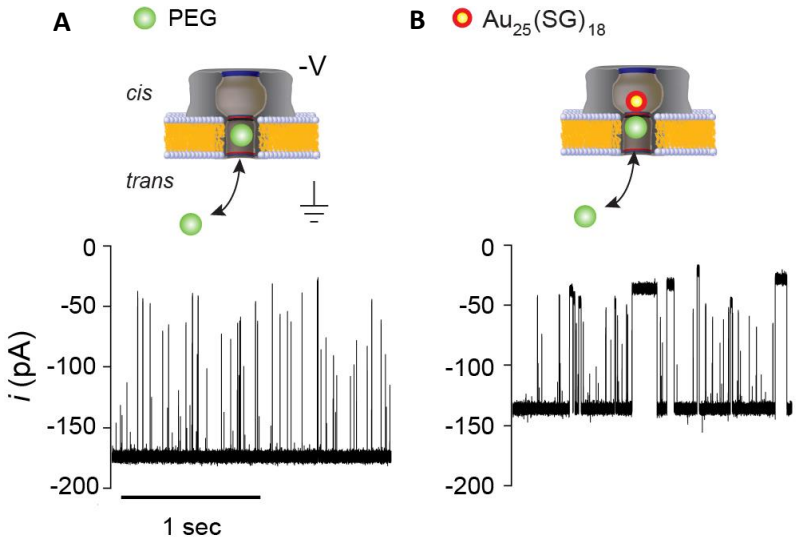

Figure 11: PEG and Cluster Trace Comparison: Current traces with and without a cluster in the pore demonstrate an increase in the PEG residence times inside a gold-cluster occupied αHL pore. (A) The empty pore exhibits an open state current i_{open}(-50 mV) = (-174.0 ± 2.7) pA. PEG molecules enter the pore at a rate of k_{on}(-50 mV) = (11.5 ± 0.1) s^{-1} and yield short lived current blockades. (B) When a cluster enters the *cis* side of the pore the current is reduced to i_{gold}(-50 mV) = (-136.5 ± 2.6) pA. With the negatively charged gold cluster in the pore, the cationic PEG molecules[35] yield longer-lived current blockades. All reported uncertainties are ± 1 S.D.

Molecular dynamics simulations have shown that PEG coordinates K^+ cations to form planar crown-ether like structures in high ionic strength solutions.[35] One possible explanation for the increased PEG residence times is that the anionic cluster interacts with the cationic PEG to create an energetically favored configuration for the PEG in the pore. Further study is required to fully understand why PEG residence times are increased with a cluster present. The

purpose of this work is to study the effects of the increased residence time on the sensing capabilities of the pore.

4.2.2 Mean Resident Time for 3.5M KCl Comb

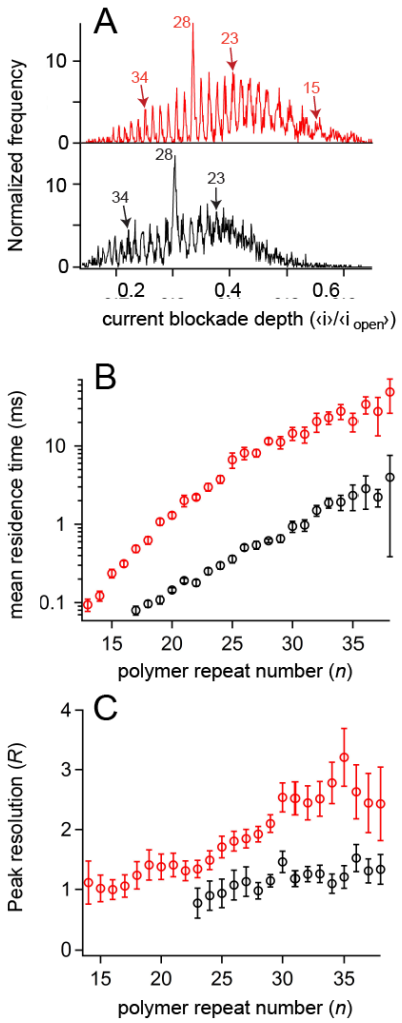

Figure 12: PEG and Cluster Comb Analysis: PEG-induced current blockade distributions, mean residence time distributions and current blockade peak resolution for PEG molecules with (red) and without (black) clusters in the pore. (A) The distribution of normalized PEG current blockades yields peaks corresponding to different sized PEG molecules.[14,15] The large peak in both distributions corresponds to the monodisperse n=28 PEG that calibrates the polymer repeat number for all peaks.[14] (B) This data was recorded with a -50 mV applied transmembrane potential (*trans* side referenced to ground) on a single pore fluctuating between the cluster-occupied and open pore states. The solution conditions were identical to those used in Fig. 11. The cluster free and cluster occupied distributions were calculated from 5443 and 5575 events respectively. All error bars correspond to ± 1 S.D. (C) The increased residence time yields narrower peaks with higher resolution (R_n = 1.18 (μ_n – μ_{n+1})/(F_n + F_{n+1})). The peak fitting

algorithm did not converge for peaks corresponding to $n < 23$ in the open pore configuration. Baseline resolution corresponds to $R \approx 1.5$.[36]

Figure 12 verifies that the gold cluster improves the SMMS analysis of a polydisperse mixture of PEG in 3.5 mol/L KCl solution. All data was taken and analyzed using a single αHL pore. In Figure 12A shows the histograms of the normalized, PEG induced, current blockades, the two combs represent the gold blocked state, in red, and the unblocked state, in black. Each peak corresponds to a PEG molecule with n monomer repeat units.[14,15] The largest peak, n = 28, is used as a marker to help distinguish between the different PEG molecules. The number and range of resolvable peaks appears greater in the gold trapped distribution (n = 13-38) than the open pore distribution (n = 23-38). The slight shift in peaks between the two distributions is expected because the gold cluster changes the effective size of the nanopore sensing volume.[15,33,**Error! Bookmark not defined.**,37] Figure 12B we take each of the comb peaks and calculate the average residence time each of the PEG molecules in the blocked and unblocked states. Gold-clusters bound to the pore increase the mean PEG residence time by roughly an order of magnitude. By introducing the gold clusters the peaks in the combs have become more resolved compared to the open state. Therefore, by increasing the residence time as shown in Fig. 12b leads to narrower peaks in the current blockade distribution as shown in Fig. 12a. This has increase the resolution of the peaks across the comb. Figure 12C shows the resolution is improved across the entire range of measurable peaks. For peaks of identical height, the lowest possible resolution for separating two adjacent peaks is 0.5 and baseline resolution is expected for $R \gtrsim 1.5$.[36] By accurately determining the resolution limit of our detection system we hope to improve our nanopore based detection system for other single molecule analysis.

4.2.3 Mean Residence time for PEG-28 at Varying Molar Concentrations

Another aspect we can change to improving the range and resolution of the current blockade distribution, the cluster induced enhancement could also be to change the concentration of analyte in the buffer. By changing the concentration of the nanopore sensing system that require the use of proteins which do not perform well in high salt concentrations, such as sequencing applications.[13,38,39] Most proteins can only function in physiological conditions ([KCl] ≲ 0.2 mol/L).[38,39]

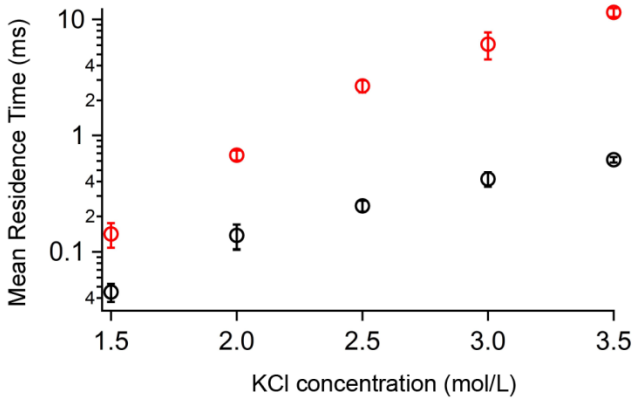

Figure 13: PEG and Cluster Mean Residence Time in Varying Salt Concentrations: The metallic clusters induce a residence time increase over a large range of KCl concentrations. The mean residence time for monodisperse PEG *n* = 28 molecules in the pore both with (red circles) and without (black circles) a gold cluster present. For concentrations 1.5 mol/L, 2.0 mol/L and 2.5 mol/L the measurements were performed with a monodisperse PEG mixture (PEG 28 at 5 μmol/L). The 3.0 mol/L and 3.5 mol/L data was recorded in the polydisperse PEG mixture described in the text. The applied transmembrane potential was -50 mV for all data shown. For each KCl concentration, data was recorded with the same pore. The error bars on all figures correspond to ± 1 S.D.

Figure 13 shows the mean residence time for *n* = 28 PEG both with and without gold clusters in the pore over a range of different KCl concentration. The PEG residence time is observed over the entire range of KCl concentrations. The residence time is improved across the

salt solutions allowing for lower KCl concentrations to achieve a particular PEG residence time. For example, the mean residence time for n = 28 PEG in 3.5 mol/L KCl ((0.62 ± 0.03) ms) is equivalent to the mean residence time in 2.0 mol/L KCl with a cluster in the pore ((0.67 ± 0.07) ms). To decrease the electrolyte concentration to 1.0 mol/L and lower a higher bandwidth detector and improved signal processing algorithms[40] are needed to obtain physiologically relevant values.

Conclusion

In summary, we set out to show that a nanopore sensing system could be used to identify, characterize, and classify water soluble ligand protected clusters on an individual level. These $Au_{25}(SG)_{18}$ clusters have been found to be negatively charged by the all points histogram under positive and negative charge. The *cis* entrance studies showed the clusters lead to a sharp peak in the blockade distribution, which could be used to size the particles. The residence time of the clusters showed an extended trapping time for particles in the pore. This could lead to further analysis of a single cluster.

After using the nanopore system to characterize the clusters, we then showed these cluster could be used to improve single molecule detection. The clusters interacted with the PEG molecules which increased their residence time in the pore. This slowdown increased the resolution and range in which an αHL pore can sense. This may provide a solution to lower salt concentrations which more closely resemble physiological conditions. Future studies will look at varying charged clusters, varying charged polymers, and adjusting the pH of the solution to increase the efficacy.

References

[1] Siegel, R. W. Nanophase materials: synthesis, structure, and properties,. In F.E. Fujita(ed), Springer Series in Material Science, Berlin Heidelberg, Springer-Verlag, 65-105. (1994).

[2] M. Burst, M. Walker, D. Bethell, D. J. Schiffrin and R. Whyman, J. Chem Soc., Chem. Commun. 801 (1994).

[3] R. Sardar, A. M. Funston, P. Mulvaney, and R. W. Murray, Langmuir. 25, 13840 (2009).

[4] Gutfleisch, O., Willard, M. A., Brück, E., Chen, C. H., Sankar, S. G. and Liu, J. P., Magnetic Materials and Devices for the 21st Century: Stronger, Lighter, and More Energy Efficient. Adv. Mater., 23: 821–842. (2011).

[5] B. F. Johnson and J. S. mcIndoe, Coord. Chem. Rev. **200-202**, 901, (2000).

[6] B. M. Quinn, P. Liljeroth, V. Ruiz, T. Laaksonen, and K. Kontturi, J. Am. Chem. Soc. **125**, 6644 (2003).

[7] M. A. H. Muhammed and T. Pradeep, Chem. Phys. Lett. **449**, 186, (2007).

[8] Farzin Haque, Jinghong Li, Hai-Chen Wu, Xing-Jie Liang, Peixuan Guo, Solid-state and biological nanopore for real-time sensing of single chemical and sequencing of DNA, Nano Today, Volume 8, Issue 1, 56-74 (2013).

[9] H.M. van den, A. R. Hall, M. Y. Wu, H. W. Zandbergen, C. Dekker, N. H. Dekker, Nanotechnology 21 (2010) 115304.

[10] H. Kwok, K. Briggs, V. Tabard-Cossa, Nanopore Fabrication by Controlled Dielectric Breakdown., PLoS ONE, 9(3): e92880 (2014).

[11] Kasianowicz JJ, Robertson JWF, Chan ER, Reiner JE, Stanford VM Nanoscopic Porous Sensors. Ann. Rev. Analy. Chem., **1**: 737–766. (2008).

[12] DeBlois R. W., Bean. C. P., Counting and Sizing of Submicron Particles by the Resistive Pulse Technique., **41**, 909 (1970).

[13] Kumar, Shiv, Tao, Chuanjuan, Chien, Minchen, Hellner, Brittney, Balijepalli, Arvind, Robertson, Joseph W. F., Li, Zengmin, Russo, James J., Reiner, Joseph E., Kasianowicz, John J., Ju, Jingyue, PEG-Labeled Nucleotides and Nanopore Detection for Single Molecule DNA Sequencing by Synthesis, Sci. Rep. (2012).

[14] Robertson, J. W. F.; Rodrigues, C. G.; Stanford, V. M.; Rubinson, K. A.; Krasilnikov, O. V. ; Kasianowicz, J. J. Single-Molecule Mass Spectrometry in Solution Using a Solitary Nanopore. Proc. Natl. Acad. Sci. U.S.A. 104, 8207-8211 (2007).

[15] Reiner, J. E.; Kasianowicz, J. J.; Nablo, B. J.; Robertson, J. W. F. Theory for Polymer Analysis Using Nanopore-Based Single-Molecule Mass Spectrometry. Proc. Natl. Acad. Sci., 107, 12080-12085 (2010).

[16] Talaga, D. S.; Li, J. Single-Molecule Protein Unfolding in Solid State Nanopores. J. Am. Chem. Soc., **131**, 9287-9297 (2009).

[17] Heaven, M. W.; Dass, A.; White, P. S.; Holt, K. M.; Murray, R. W. J. Am. Chem. Soc., **130**, 3754–3755 (2008).

[18] Robertson, J., Kasianowics, J., Banerjee, S., Analytical Approaches for Studying Tansporters, Channels and Porins, Chem. Rev., **112**, 6227-6249 (2012).

[19] Bhakdi, S., Tranum-Jenson, J., Microbiol. Rev., 55, 733 (1991).

[20] Song, L., Hobaugh, M., Shustak, C., hagan, B., and Gouaux, J., Structure of Staphylococcal a-Hemolysin, a Heptameric Transmembrane Pore, Science, **274**, 1859-1866 (1996).

[21] Structure Population in Thiol-Passivated Gold Nanoparticles D. Zanchet, B. D. Hall, and, and D. Ugarte The Journal of Physical Chemistry B, 104 (47), 11013-11018 (2000).

[22] Aksimentiev, A., Schulten, K., Imaging α-Hemolysin with Molecular Dynamics: Ionic Conductance, Osmotic Permeability, and the Electrostatic Potential Map, Biophys. Jour., **(6), 3745-3761 (2005)

[23] DeGuzman, V., Lee, C., Deamer, D., and Vercoutere, W., Sequence-dependent gating of an ion channel by DNA hairpin molecules, Nucleic Acids Res. **34**: 6425–6437 (2006).

[24] de Zoysa, R. S. S., Krishantha, D. M. M., Zhao, Q., Gupta, J. and Guan, X., Translocation of single-stranded DNA through the α-hemolysin protein nanopore in acidic solutions. ELECTROPHORESIS, 32: 3034–3041(2011).

[25] Wright, W. B., The Crystal Structure of Glutathione, Acta Cryst., **11**, 632 (1958).

[26] U.S. Patent, Akihiro Mizutani, "Complexes of polysaccharides or derivatives thereof with reduced glutathione and process for preparing said complexes." U.S. Patent US4009264, issued February, (1971).

[27] Zhu, M. Aikens, C. M., Hollander, F. J., Schatz, G. C., and Rongchao, J., Correlating the structure of A Thiol-Protected Au25 Cluster and optical Properties, J. AM. Chem. Soc., 130, 5883-5885 (2008).

[28] N. Spear, S.D. Aust, Thiol-mediated NTA-Fe(III) reduction and lipid peroxidation Arch. Biochem. Biophys., **312**, 198–202 (1994).

[29] Liu, Y., Tsunoyama, H., Akita T., and Tsukuda, T., Efficient and selective epoxidation of styrene with TBHP catalyzed by Au25clusters on hydroxyapatite, R. Soc. Chem., 46, 550-552 (2010).

[30] Negishi, Y.; Nobusada, K.; Tsukuda, T. Glutathione-Protected Gold Clusters Revisited: Briding the Gap between Gold(I)-Thiolate Complexes and Thiolate-Protected Gold Nanocrystals. J. Am. Chem. Soc., **127**, 5261-5270 (2005).

[31] Huang, W.; Pal, R.; Wang, L-M.; Zeng, X. C.; Wang, L-S. Isomer identification and resolution in small gold clusters. J. Chem. Phys., **132**, 054305 (2010).

[32] Aksimentiev, A.; Schulten, K. Imaging α-Hemolysin with Molecular Dynamics: Ionic Conductance, Osmotic Permeability, and the Electrostatic Potential Map. Biophys. J., **88**, 3745-3761 (2005).

[33] Robertson, J. W. F.; Kasianowicz, J. J.; Reiner, J. E. Changes in ion channel geometry resolved to sub-ångström precision via single molecule mass spectrometry. J. Phys.: Condens. Matter, **22**, 454108 (2010).

[34] E. C. Gregg and K. David Steidley, Electrical Counting and Sizing of Mammalian Cells in Suspension, Biophys. Journal, **5**, 393-405 (1965)

[35] Balijepalli, A.; Robertson, J. W. F.; Reiner, J. E.; Kasianowicz, J. J.; Pastor, R. W. Theory of Polymer-Nanopore Interactions Refined Using Molecular Dynamics Simulations. J. Am. Chem. Soc., **135**, 7064-7072 (2013).

[36] Felinger, A. Critical Peak Resolution in Multicomponent Chromatograms. Anal. Chem., **69**, 2976-2979 (1997).

[37] Krasilnikov, O. V.; Rodrigues, C. G.; Bezrukov, S. M. Single Polymer Molecules in a Protein Nanopore in the Limit of a Strong Polymer-Pore Attraction. *Phys. Rev. Lett.*, ***97***, 018301 (2006).

[38] Clarke, J.; Wu, H.-C.; Jayasinghe, L.; Patel, A.; Reid, S.; Bayley, H. Continuous Base Identification for Single-Molecule Nanopore DNA Sequencing. *Nat. Nanotech.*, ***4***, 265-270 (2009).

[39] Lieberman, K. R.; Dahl, J. M.; Mai, A. H.; Akeson, M.; Wang, H. Dynamics of the Translocation Step Measured in Individual DNA Polymerase Complexes. *J. Am. Chem. Soc.*, ***134***, 18816-18823 (2012).

[40] Balijepalli, A.; Ettedgui, J.; Cornio, A. T.; Robertson, J. W. F.; Cheung, K. P.; Kasianowicz, J. J.; Vaz, C. Quantifying Short-Lived Events in Multistate Ionic Current Measurements. *ACS Nano*, ***8***, 1547-1553 (2014).